Understanding 4D seismic inversion results through the analysis of the water breakthrough in a clastic reservoir in Campos Basin

Ekaterina Kneller[1], Ulisses Correia[1], Ruan Giacomini Couto[2], Paula Dariva dos Reis[2], Paulo de Oliveira Maciel Junior[2], Wilson Lisboa Ramos Filho [2]. [1]CGG, [2]Petrobras.

This paper was prepared for presentation during the 18th International Congress of the Brazilian Geophysical Society held in Rio de Janeiro, Brazil, 16-19 October 2023.

Abstract

4D seismic inversion has increased potential to enable a quantitative interpretation of reservoir behavior during production. The objective of this study is to quantify the reservoir rock property changes through the analysis of 4D effects detectable on seismic. We analyze increases or decreases in impedances from baseline to monitor, where the differences account for production effects between the acquisition times. The inversion workflow, applied in a turbidite reservoir from the Campos Basin Brazil, makes it possible to analyze and delineate the waterfront. We analyzed the fluids contact movement and water breakthrough related structures i.e., fingering. Despite the benefits of this approach, there is some uncertainty in the results such as residual sidelobes. A forward modeling exercise can help the interpretation of the presence of water, represented by the impedance hardening effect.

Introduction

Several studies have been carried out with 4D seismic inversion to help understanding the reservoir behavior from the standpoint of dynamic properties (e.g., Johnston, 2013; Calvert et al., 2016; Blanchard et al., 2021). In particular, they provide more information on the impact of production on the reservoir rock properties and the possibility of inferring the fluid movement during this period.

The detectability of the production-induced 4D effects during the reservoir production plays an extremely important role in advanced reservoir characterization. Thus, it is important to be able to quantify those changes. The knowledge about preferential paths of fluid movement and the identification of non-drained zones facilitates an optimization of and increase in the economic efficiency of future production (e.g., Johnston, 2010). However, the reservoir rock properties that control the reservoir behavior are often inaccessible directly from the 4D seismic data alone. A rock physics analysis based on well-calibrated petro-elastic models enables one to build a direct link between seismic and petrophysical properties of the reservoir (Allo et al., 2011).

This work showcases a 4D study for the reservoir characterization of an oilfield in the Campos Basin, in the southeastern Brazilian continental margin. The production zone contains Maastrichtian turbidite sandstone reservoirs deposited in a deep marine environment. These reservoirs have high average porosity and absolute permeability, with an oil gravity less than 20 API.

In this reservoir characterization work, the results of 4D seismic inversion were compared to petro-elastic models. It was possible to highlight the main benefits from 4D seismic inversion and outline some of the associated limitations.

Method and application

We used 4D inversion method to conduct analysis on the changes in rock properties during production (Lafet et al., 2008). The main purpose of the 4D inversion is to derive a model of the changes in the elastic properties of the reservoir from the seismic amplitude variations between vintages. The 4D inversion workflow consists of several stages, including seismic data preconditioning, wavelet extraction, low-frequency model building, and simultaneous 3D inversion (Coulon et al., 2006), from which we build the initial model for the 4D inversion itself.

The simultaneous 4D inversion workflow requires initial models for the Base and Monitor (Figure 1), which are used to invert the Base and Monitor seismic data, respectively. The initial model is perturbed iteratively until a global solution is found. This solution optimizes for all the vintages the match between the seismic angle stacks and the corresponding synthetics, which are computed by the convolution of the wavelet with reflectivity traces derived using either the full Zoeppritz or the Aki-Richards equation. This inversion has a multi-vintage and multi-angle stacks cost function to be minimized based on a Simulated Annealing technique. These terms include (1) the residual energy from each angle stack and vintage, (2) the distance from an initial model, and (3) lateral and vertical constraints to control the noise between traces. In this method, it is also possible to control the level of 4D coupling between inverted elastic properties. The simultaneous inversion performs multi-vintage perturbations jointly for P-Velocity, S-Velocity, and Density during the Simulated Annealing minimization and accepts them or rejects globally.

Although the inversion was performed in the elastic domain and both acoustic and shear impedance ratio were obtained in this project, here we only analyze the acoustic impedance ratio result. This decision was made for two

reasons. First, the expected production effects are mostly water saturation changes, which are interpretable in the acoustic impedance domain. Second, the 4D changes of shear impedance are more sensitive to noise, which increases the uncertainty in their interpretation.

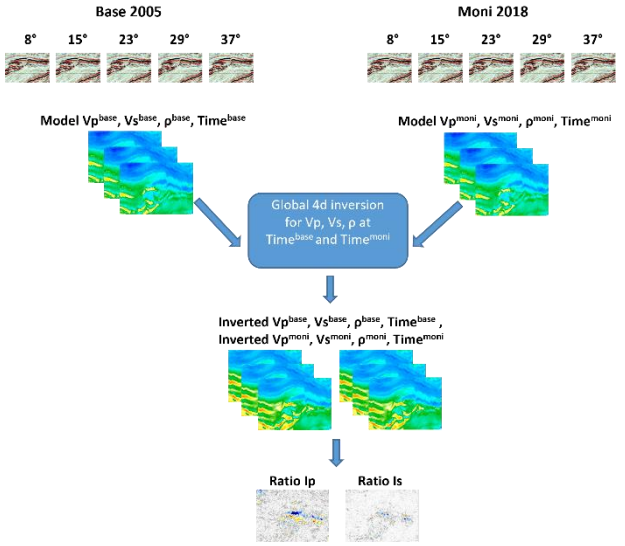

Figure 1. Simultaneous 4D seismic inversion of multiple seismic vintages and angle stacks with coupling of inverted attributes between successive surveys.

To improve the seismic quality for the target reservoir, the angle stacks of Base and Monitor have been preconditioned to increase the signal-to-noise ratio and improve the residual time misalignment between angle stacks and vintages. Figure 2A shows the 4D seismic difference calculated by subtracting the original amplitudes of the Base near-angle stack from the Monitor near-angle stack. Figure 2B shows the same 4D difference after preconditioning, increasing the signal-to-noise ratio and, thus, making the 4D anomalies clearer.

In our case study, the same initial models of elastic properties have been used to invert the Base and the Monitor.

Due to the difference of low-frequency content observed between Base and Monitor vintages, different wavelets for Base and Monitor were utilized in the 4D inversion (Kneller et al., 2021). This resulted in less 4D noise and allowed for better mapping of the main anomaly.

Figure 2C shows the acoustic impedance ratio from the 4D inversion. The main hardening anomaly, related to the increase of impedance, can be seen in blue. The position of the section can be seen on Figure 3, from south to north.

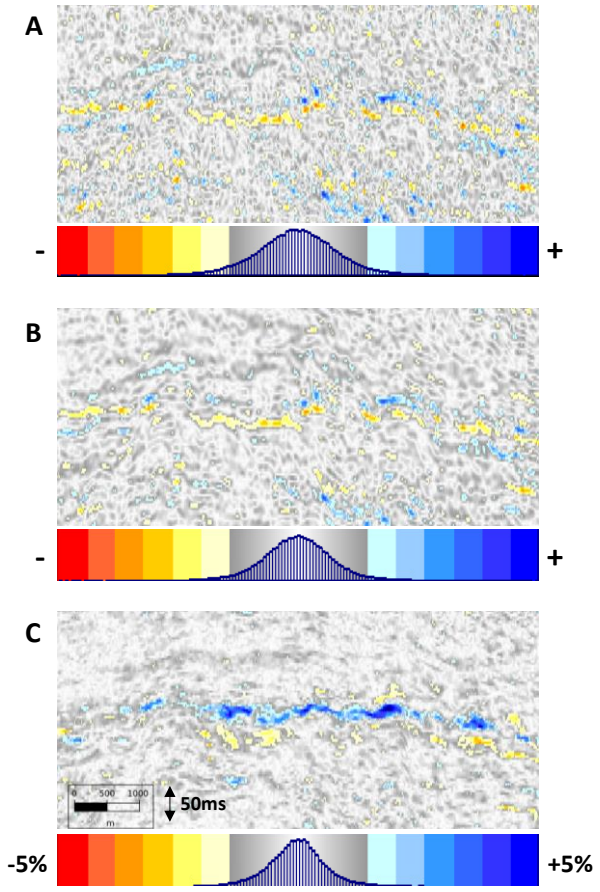

Figure 2. Comparison between the 4D seismic difference for the near-angle stack before preconditioning (A), after preconditioning (B) and inverted 4D acoustic impedance ratio (C). The red line on Figure 3 shows the location of the section line, south to north.

The spatial extension of the main hardening anomaly was extracted as the maximum acoustic impedance ratio in a time window around the top of reservoir (Figure 3B). It is compared with the quadrature attribute of the 4D seismic difference extracted using the same time window (Figure 3A). The inversion result shows better continuity and allows better delineation of the main anomaly.

4D acoustic impedance ratio modeling

We applied the following petro-elastic modeling concepts (Allo et al., 2011) with the objective to obtain a reference for further analysis of 4D anomalies observed from seismic.

The dry rock bulk and shear moduli properties for Base and Monitor were calculated at well locations (Batzle and Wang, 1992) using a petro-elastic model calibrated at wells. Next, these values have been kriged inside the reservoir grid, and the acoustic impedance for Base and

Monitor were calculated to derive the impedance ratio. Figure 3C shows a map of the maximum synthetic acoustic impedance ratio in the same time window as the maps of Figure 3A and Figure 3B.

We can observe that the contour of the main hardening anomaly on synthetic (Figure 3C) is globally similar with the inversion result (Figure 3B). Nevertheless, seismic data seem to bring many of additional details in the delineation of the anomaly compared to the synthetic, which was based on simple assumptions and used kriging technique as an interpolation method.

both wells PROD1 and PROD2 (dashed line Figure 5C and Figure 6C).

Despite the confidence in the inversion results drawn from the analysis of the hardening anomaly, some significant negative impedance ratio can be observed. These zones were interpreted as effects of bandlimited side lobes but can also be interpreted as softening anomalies. Considering such softening was not predicted by synthetic modeling, we decided to frequency filter the synthetic acoustic impedance ratio to compare the response with the attributes from seismic. First, a high-cut frequency filter

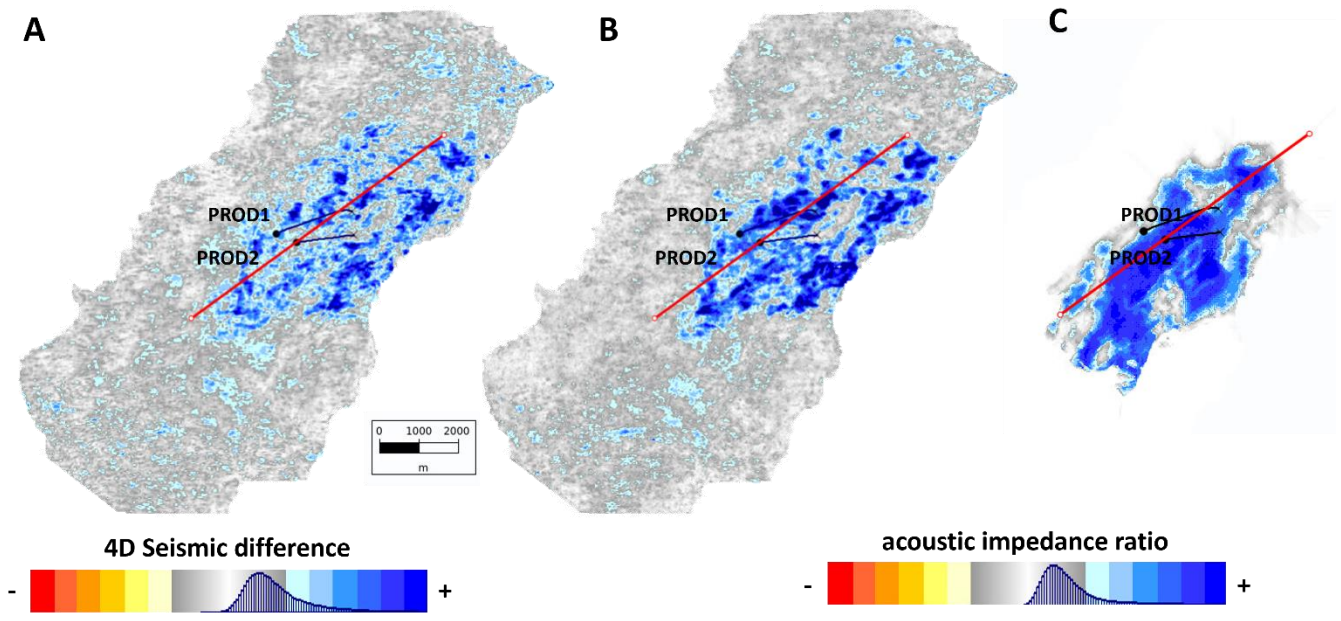

Figure 3. Extracted maps of the maximum in a time window selected to catch the main hardening anomaly, from the 4D seismic difference near angle stack quadrature of the preconditioned seismic data (A), the inverted acoustic impedance ratio (B), the synthetic acoustic impedance ratio (C).

4D Interpretation and discussion

The 4D response from these turbidite reservoirs enables us to infer the movement of the fluids during the time of production, from 2005 to 2018, which correspond to the Base and Monitor surveys, respectively. The hardening anomalies (impedance increase) detected from seismic data agree with the current water saturation of the producing wells (PROD1 and PROD2), which have been operating since 2011. More specifically, the hardening anomalies may be associated to (1) a relative rise in the oil-water contact due to fluid substitution – water replacing oil and (2) slight water fingering occurring around the well. The rise in the oil-water contact is corroborated by the anomaly spreading above the original oil-water contact for

designed using the seismic data was applied to the impedance ratio modeled cube (Figure 4B). In zones where the water layer is thin, the anomaly either disappears or appears thicker than it is in the original model (blue arrow on Figure 4).When we further apply a low-cut filter on the modeled impedance ratio, with the objective to understand the impact on the results, sidelobes appear as softening anomalies around the main hardening anomaly (Figure 4C). Furthermore, with the help of the synthetic impedance ratio from the petro-elastic modeling, we identified a maximum observable thickness for the water anomaly linked to the lack of low frequencies. We could observe that in locations where the thickness of the anomaly is inferior to this limit, the side lobes are located closely to the main hardening anomaly – as shown by the red arrow at the Figure 4C. Also, in zones where the water breakthrough thickness anomaly is superior to the limit, the side lobes, observed as softening anomalies, are

located with some offset above the main hardening anomaly – as shown with the green arrow at the Figure 4C.

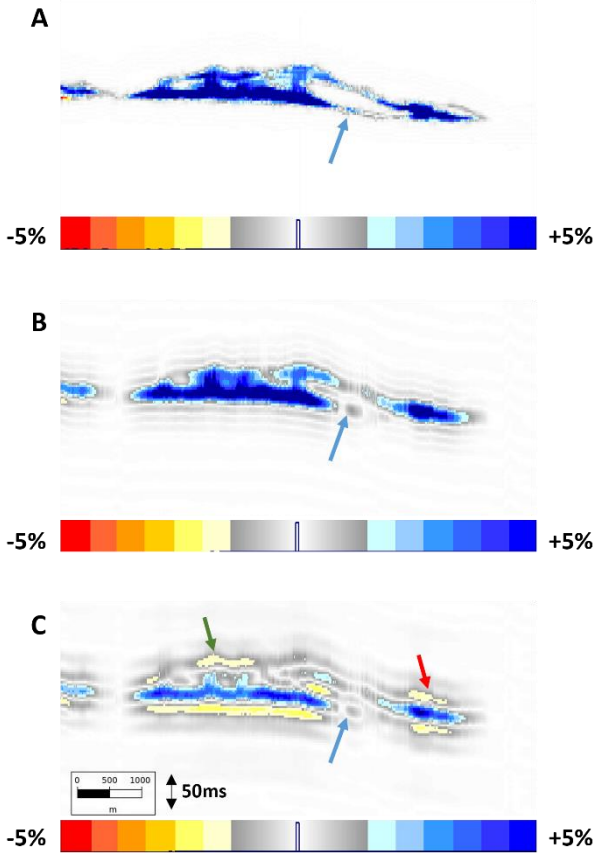

Figure 4. Comparison of the petro-elastic modeling depicting the synthetic acoustic impedance ratio with bandwidth 0-125Hz (A), synthetic acoustic impedance ratio with bandwidth 0-30 Hz (B), and the synthetic acoustic impedance ratio with bandwidth 6-30 Hz (C). The red line on Figure 3 shows the location of the section line, south to north.

This empiric exercise helped in understanding of the 4D inversion result. In Figure 5, we analyze the inverted acoustic impedance ratio (Figure 5C) with the support of the synthetic forward modeling result (Figure 5A) and the bandlimited synthetic forward modeling result (Figure 5B). The lateral extension of the hardening anomaly is similar for all three images, but the height of the anomaly in the full bandwidth synthetic acoustic impedance ratio is different compared to the inverted one. Around the kick-off point of the well PROD1, blue arrow in the Figure 5A, we observe an anomaly in the synthetic acoustic impedance ratio not detected in the inverted one (Figure 5C). We can observe more similarity between the inverted acoustic impedance ratio (Figure 5C) and the limited frequency bandwidth synthetic acoustic impedance ratio (Figure 5B). On the inversion results, we can also observe some relative change of the vertical position of the side lobes compared to the main hardening anomaly, as highlighted at the synthetic exercise. This provides confirmation of the side lobe interpretation.

The analysis of well PROD1 suggested the presence of two zones where the water saturation increased – the deeper zone with a higher water column and the shallower zone with fewer changes in water height. These zones may be connected through a high permeability layer. In the inversion result, we can observe a single hardening anomaly. The second thinner anomaly seen on the synthetic may be due to water fingering, and the connection zone is not visible on the inversion result because of the limited frequency band and noise presence.

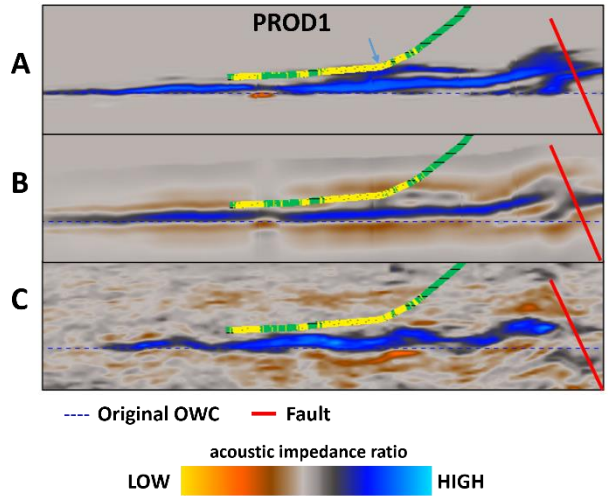

Figure 5. Cross-section through the producing well PROD1 for the full bandwidth synthetic acoustic impedance ratio (A), 6-30 Hz synthetic acoustic impedance ratio (B), and inverted acoustic impedance ratio (C).

In the full bandwidth synthetic acoustic impedance ratio for the well PROD2 (Figure 6A), we can also observe anomalies associated with water replacing oil due to production. Both the rise in the oil-water contact and water fingering through more permeable layers within the reservoir can be observed. When limiting the frequency bandwidth (Figure 6B), we miss the water fingering and the connection zone. The limited frequency of inversion result does not allow us to interpret these features (Figure 6C). Without integrating multidisciplinary knowledge in this field, we might have a different and, perhaps, misleading interpretation of the water movement. It is important to understand that both types of information showed on Figure 5 and Figure 6 contain some uncertainty. The synthetic acoustic impedance ratio relies on series of assumptions with high uncertainty far from wells. The inverted acoustic impedance contains uncertainty related

to the 4D seismic noise and the limited bandwidth. For example, we can see that the synthetic model assumes the fault permeable and highlights an anomaly at the right side of the fault. In contrast, inversion does not show such anomaly, which can mean either absence of the waterfront there, low intensity, or height below the resolution.

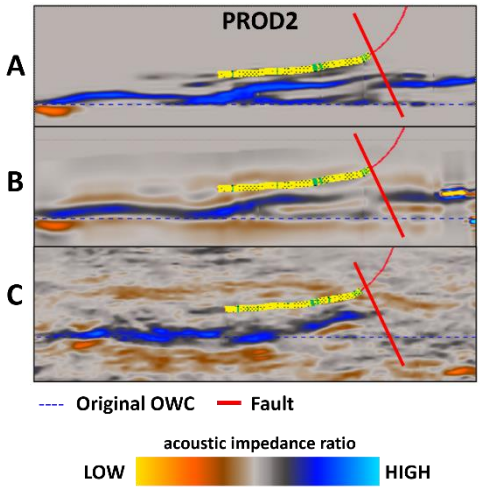

Figure 6. Cross-section through the producing well PROD2 for the full bandwidth synthetic acoustic impedance ratio (A), 6-30 Hz synthetic acoustic impedance ratio (B), and inverted acoustic impedance ratio (C).

From the production of the reservoir, we expect changes in water level. The hardening effects interpreted from the inverted impedance ratio can partially quantify such water bodies. Thus, it is important to try and quantify this height to further improve the 4D analysis of the impact of production. To do so, we applied a 1.5% cutoff to the acoustic impedance ratio values in the depth domain. Next, we extracted the thickness of this zone (Figure 7). As expected, the spatial distribution of the water height map is similar to the distribution of the maximum acoustic impedance ratio map shown in Figure 3B. We can also identify zones with larger changes in water level which are compatible with the prior knowledge about reservoir.

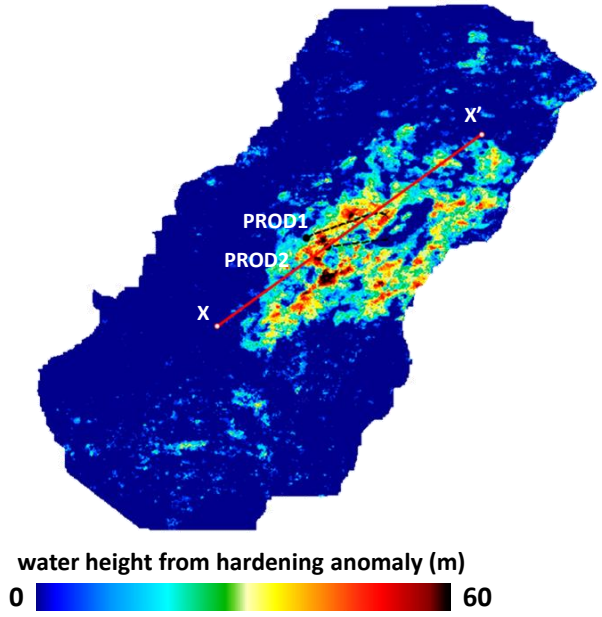

Figure 7. Map showing the variation of the water height, extracted from the impedance hardening anomaly.

Conclusions

These results demonstrate the relevance of 4D inversion-based attributes to better understand the water breakthrough in the producing wells and, potentially, to help improve production by water injection. We have demonstrated how the interpretation of inversion results can benefit from the support of synthetic modeling to characterize the uncertainty contained in the inversion result. This inversion-based quantitative interpretation provides solid reservoir characterization insights to support the oil field development activities.

Acknowledgments

The authors thank Petrobras and CGG for permission to publish this article. All colleagues involved in the 4D inversion project are also acknowledged for their insightful contribution.

References

Allo, F., Coléou, T., Colnard, O., Machecler, I., Dillon, L., Schwedersky., G., Nunes, C., Abreu, E. 2011. Petrophysical Seismic Inversion over an offshore carbonate field. 12th International Congress of the Brazilian Geophysical Society & EXPOGEF, Rio de Janeiro, Brazil, 15–18 August 2011, https://doi.org/10.1190/sbgf2011-281.

Batzle, W., Wang., Z. 1992. Seismic properties of pore fluids. Geophysics, Volume 57, Issue 11, https://doi.org/10.1190/1.1443207.

Blanchard, T., Henriquel, M., Granel, J., Cherrett, A., Adeyemi, A. 2021. Is there value in 4D Elastic Inversion?. 82nd EAGE Annual Conference & Exhibition, Oct 2021, Volume 2021, p.1 – 5, https://doi.org/10.3997/2214-4609.202112857.

Calvert, M.A., Hoover, A.R., Vagg, L.D., Ooi, K.C., Hirsch, K.K. 2016. Halfdan 4D workflow and results leading to increased recovery. The Leading Edge, v. 35, n. 10, p.840-848, out. 2016. Society of Exploration Geophysicists, https://doi.org/10.1190/tle35100840.1.

Coulon, J-P., Lafet Y., Deschizeaux, B., Doyen, P.M., Duboz, P. 2006. Stratigraphic elastic inversion for seismic lithology discrimination in a turbiditic reservoir, *SEG Annual Meeting*, Expanded Abstracts, 2092-2096, New Orleans, US, https://doi.org/10.1190/1.2369949.

Johnston, D.H. 2013. Making a Difference with 4D: Practical Applications of Time-Lapse Seismic Data. In: SEG Distinguished Instructor Short Course, https://doi.org/10.1190/1.9781560803126.

Johnston, D.H., Tiwari, U., Helgerud, M.B. New opportunities from 4D seismic and lithology prediction at Ringhorne field, Norwegian North Sea. SEG Technical Program Expanded Abstracts: 4160-4164, https://doi.org/10.1190/1.3513732.

Kneller, E., Correia, U., Coulon, J.P., Oliveira, L., Maciel Junior, P.O., Ramos Filho, W.L. 2021. The impact of wavelet estimation in 4D inversion — an offshore Brazil case study. First Break, Volume 39, Issue 11, Nov 2021, p. 45 – 51, https://doi.org/10.3997/1365-2397.fb2021082.

Lafet, Y., Roure, B., Doyen, P.M., Bornard, R., Buran, H., 2008. Global 4-D seismic inversion and time-lapse fluid prediction. SEG Technical Program Expanded Abstracts 2009. https://doi.org/10.1190/1.3255666.